Cerebral Cortex, April 2020;30: 2673–2689

doi: 10.1093/cercor/bhz268
Advance Access Publication Date: 9 December 2019
Original Article

ORIGINAL ARTICLE

Differential White Matter Maturation from Birth to 8 Years of Age

Qinlin Yu[1,2], Yun Peng[3], Huiying Kang[3], Qinmu Peng[1,2], Minhui Ouyang[1], Michelle Slinger[1], Di Hu[3], Haochang Shou[4], Fang Fang[5,6,7,8] and Hao Huang[1,2]

[1]Department of Radiology, Children's Hospital of Philadelphia, Philadelphia, PA 19104, USA, [2]Department of Radiology, Perelman School of Medicine, University of Pennsylvania, Philadelphia, PA 19104, USA, [3]Department of Radiology, Beijing Children's Hospital, Capital Medical University, National Center for Children's Health, Beijing 100045, China, [4]Department of Biostatistics and Epidemiology, Perelman School of Medicine, University of Pennsylvania, PA, USA, [5]School of Psychological and Cognitive Sciences and Beijing Key Laboratory of Behavior and Mental Health, Peking University, Beijing 100871, China, [6]Key Laboratory of Machine Perception, Peking University, Beijing 100871, China, [7]Peking-Tsinghua Center for Life Sciences, Peking University, Beijing 100871, China, and [8]PKU-IDG/McGovern Institute for Brain Research, Peking University, Beijing 100871, China

Address correspondence to Hao Huang, Department of Radiology, Children's Hospital of Philadelphia, Perelman School of Medicine, University of Pennsylvania, PA, USA. Email: huangh6@email.chop.edu. or Fang Fang, School of Psychological and Cognitive Sciences, Peking University, Beijing, P. R. China. Email: ffang@pku.edu.cn
Qinlin Yu and Yun Peng contributed equally to this work

Abstract

Comprehensive delineation of white matter (WM) microstructural maturation from birth to childhood is critical for understanding spatiotemporally differential circuit formation. Without a relatively large sample of datasets and coverage of critical developmental periods of both infancy and early childhood, differential maturational charts across WM tracts cannot be delineated. With diffusion tensor imaging (DTI) of 118 typically developing (TD) children aged 0–8 years and 31 children with autistic spectrum disorder (ASD) aged 2–7 years, the microstructure of every major WM tract and tract group was measured with DTI metrics to delineate differential WM maturation. The exponential model of microstructural maturation of all WM was identified. The WM developmental curves were separated into *fast*, *intermediate*, and *slow* phases in 0–8 years with distinctive time period of each phase across the tracts. Shorter periods of the *fast* and *intermediate* phases in certain tracts, such as the commissural tracts, indicated faster earlier development. With TD WM maturational curves as the reference, higher residual variance of WM microstructure was found in children with ASD. The presented comprehensive and differential charts of TD WM microstructural maturation of all major tracts and tract groups in 0–8 years provide reference standards for biomarker detection of neuropsychiatric disorders.

Key words: 0–8 years, autism, differential maturation, diffusion tensor imaging (DTI), exponential, white matter

Introduction

During infancy and childhood, the human brain white matter (WM) undergoes significant microstructural changes (Yakovlev and Lecours 1967; Haynes et al. 2005), with dynamic axonal and myelin maturation. These WM maturational processes underlie the structural basis of emerging brain circuits critical to memory (Nagy et al. 2004; Engvig et al. 2012), attention (Tuch et al. 2005), intelligence quotient (Schmithorst et al. 2005), language (Carreiras et al. 2009; Brauer et al. 2011; Dubois et al. 2015), motor learning (Scholz et al. 2009), musical proficiency (Bengtsson et al. 2005; Hyde et al. 2006), and cognitive control (Liston et al. 2006). Dysfunction of the WM maturational processes is associated with a suite of neuropsychological disorders including schizophrenia (Shenton et al. 2001; Douaud et al. 2007; Gogtay et al. 2008; Leech and Sharp 2014), major depressive disorder (Cullen et al. 2010; Aghajani et al. 2014), bipolar disorder (Frazier et al. 2007), autism (Barnea-Goraly et al. 2004; Koldewyn et al. 2014; Ouyang et al. 2016), and attention-deficit hyperactivity disorder (ADHD) (Silk et al. 2009; van Ewijk et al. 2014). WM tracts are often categorized into commissural (interhemispheric connection), brainstem (connectivity in brainstem and cerebellum), association (corticocortical connections), limbic (connectivity in limbic system), and projection (corticospinal connections) tract groups based on the tract functions (Wakana et al. 2004). Delineation of maturational WM microstructural curves of all major WM tracts and tract groups of typically developing (TD) brain could not only reveal the spatiotemporal differential circuit formation in normal brain development, but also set the stage for understanding aberrant brain development in neurodevelopmental disorders such as autistic spectrum disorder (ASD) and developmental brain disorders in general.

Diffusion MRI, especially diffusion tensor imaging (DTI), has been widely used to quantify WM microstructure (Le Bihan et al. 2001). Water molecules tend to diffuse more freely along the WM tracts, rather than perpendicular to the tracts. These diffusion properties of water molecules around WM tracts can be measured through DTI, which uses a tensor model to measure the water diffusion in vivo. DTI-derived metrics are sensitive to WM microstructural changes during development. Fractional anisotropy (FA), ranging from 0 to 1, has been utilized to quantify the shape of the diffusion tensor (Song et al. 2002). Radial diffusivity (RD) and axial diffusivity (AD), the diffusivity measurements perpendicular to and along the diffusion tensor, are associated with myelination and axonal growth, respectively. (Song et al. 2002, 2005). Mean diffusivity (MD) quantifying the size of the diffusion tensor usually decreases during brain development (Lebel et al. 2008).

The human brain WM develops relatively fast during the first few years after birth (Mukherjee et al. 2001; Hermoye et al. 2006; Deoni et al. 2012; Geng et al. 2012; Sadeghi et al. 2013; Yu et al. 2014), then goes through a transitional stage with a relatively slower developmental rate in early childhood, and then undergoes a slower and more stable developmental period until late childhood and adolescence (Lebel et al. 2008; Westlye et al. 2010; Lebel and Beaulieu 2011; Lebel et al. 2012). Knowledge on human brain WM maturation has been obtained with DTI studies of TD brains at different age periods (Mukherjee et al. 2001; Schneider et al. 2004; Dubois et al. 2006, 2008; Hermoye et al. 2006; Lebel et al. 2008, 2012, 2017; Schmithorst et al. 2008; Westlye et al. 2010; Lebel and Beaulieu 2011; Geng et al. 2012; Sadeghi et al. 2013, 2015; Yu et al. 2014). Differential maturation was also observed across major WM tracts (Huang et al. 2006, 2009) or tract groups (Mishra et al. 2013) with these DTI measurements. All the above-mentioned findings suggest multiple characteristic maturational stages and spatiotemporally differential developmental rates from birth until end of early childhood. So far, linear (Dubois et al. 2006; Schmithorst et al. 2008; Asato et al. 2010), exponential (Mukherjee et al. 2001; Schneider et al. 2004; Lebel et al. 2008; Sadeghi et al. 2013), logarithmic (Deoni et al. 2012; Yu et al. 2014), Poisson (Lebel et al. 2012), and quadratic polynomial (Westlye et al. 2010; Lebel and Beaulieu 2011) models have been proposed to characterize maturation

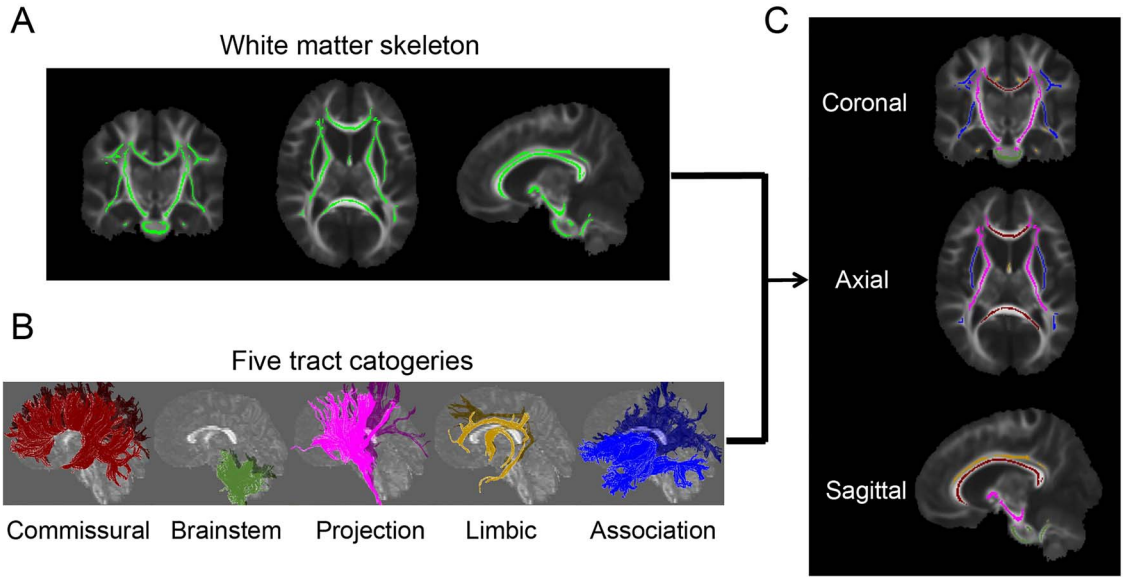

Figure 1. Parcellation of the WM skeleton into five tract groups. (*A*) The skeleton of the entire WM in coronal (left), axial (middle), and sagittal (right) view after setting the FA threshold 0.2; (*B*) 3D reconstructed commissural, brainstem, projection, limbic, and association tract groups in sagittal view; (*C*) parcellation of the WM skeleton into five tract groups with the tract group colors consistent to those shown in (*B*).

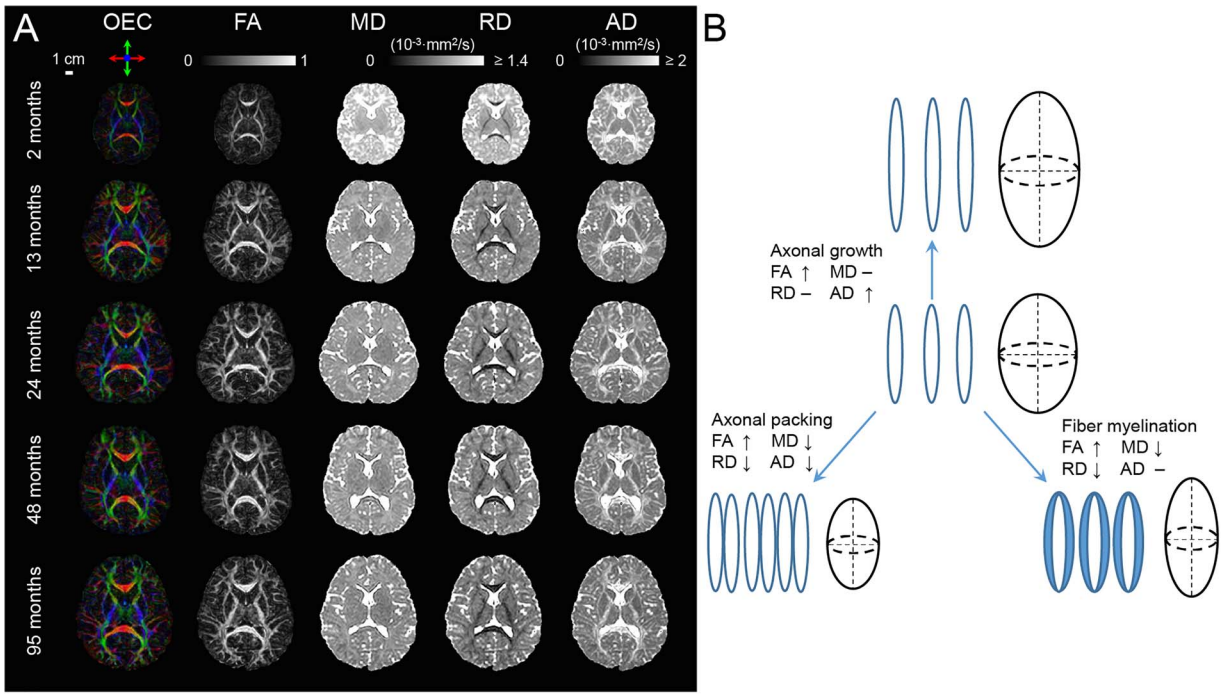

Figure 2. (*A*) Representative axial OEC, FA, MD, RD, and AD maps at the level of the internal capsule from a representative 2-, 13-, 24-, 48-, and 95-month-old child from top to bottom. (*B*) The diagram shows hypothesized association between cellular processes (axonal growth, axonal packing, and myelination) and DTI metric changes during WM development.

of WM microstructure quantified by FA measurement. Most previous DTI studies (Mukherjee et al. 2001; Hermoye et al. 2006; Huang et al. 2006; Dubois et al. 2008; Lebel et al. 2008, 2012; Deoni et al. 2012; Geng et al. 2012; Sadeghi et al. 2013; Kersbergen et al. 2014; Yu et al. 2014, 2016) delineated early WM development over relatively short periods and a limited number of WM tracts. Few of them have covered the critical age ranges of both infancy (0–2 years) and early childhood (2–8 years) which are characterized by fast and relatively slow WM maturation, respectively. In addition, similar to the growth charts of child height or weight, TD brain WM maturation charts provide reference for understanding WM aberration in children with atypical brain development. Measures such as z-score can be obtained for the test subject if WM maturation curve and standard deviations of TD brains of a very large cohort of subjects can be established. As controversial findings of increasing (Bashat et al. 2007; Weinstein et al. 2011) and decreasing (Sundaram et al. 2008; Walker et al. 2012) WM microstructural integrity in children with ASD were found in previous studies, quantifying residual variance difference between ASD and TD group (instead of measuring z scores) based on comprehensive DTI metric measurements of all major WM tracts and tract groups may offer refreshing insights into WM microstructural aberrations in children with ASD.

It is critical to establish normal charts of WM microstructural changes in 0–8 years and more importantly, to identify the distinguished developmental phases and differential development across WM tracts. Establishment of these WM maturational charts requires age coverage of both early childhood and infancy stage for appropriate maturational curve fitting, a relatively large sample number, and comprehensive quantification of all major WM tracts and tract groups. Here, we delineated WM microstructural maturation of 118 TD children aged 0.17–7.91 years with DTI metric (FA, MD, RD, and AD) measurements of all major tracts and tract groups. In addition, 31 children with ASD were recruited to assess the aberrant WM maturation with the TD WM charts as the reference.

Materials and Methods

Pediatric Subjects

Hundred and eighteen TD children (52 M/66F; mean age: 3.36 ± 2.44 years; age range: 0.17–7.91 years) and 31 children with ASD (31 M; mean age: 4.11 ± 1.42 years; age range: 2.33–7 years old) were recruited at Beijing Children's Hospital. The clinical history of each child in the TD cohort was carefully inspected by pediatric radiologists (H.K. and D.H.) to rule out developmental abnormalities. The exclusion criteria included known nervous system disease and/or a history of psychiatric, neurodevelopmental, or systemic illness. The children in the TD cohort were referred to MR imaging in the case of seizures with fever, sexual precocity, intermittent headache, short stature, or convulsion. No brain abnormalities were detected on the MRI scans of the TD children. This study was approved by Institutional Review Board, and written informed consent of every TD subject and every child with ASD was obtained from each subject's parent.

The details of diagnosis of children with ASD and evaluation of differences of residual variances of DTI measurements between TD children and children with ASD

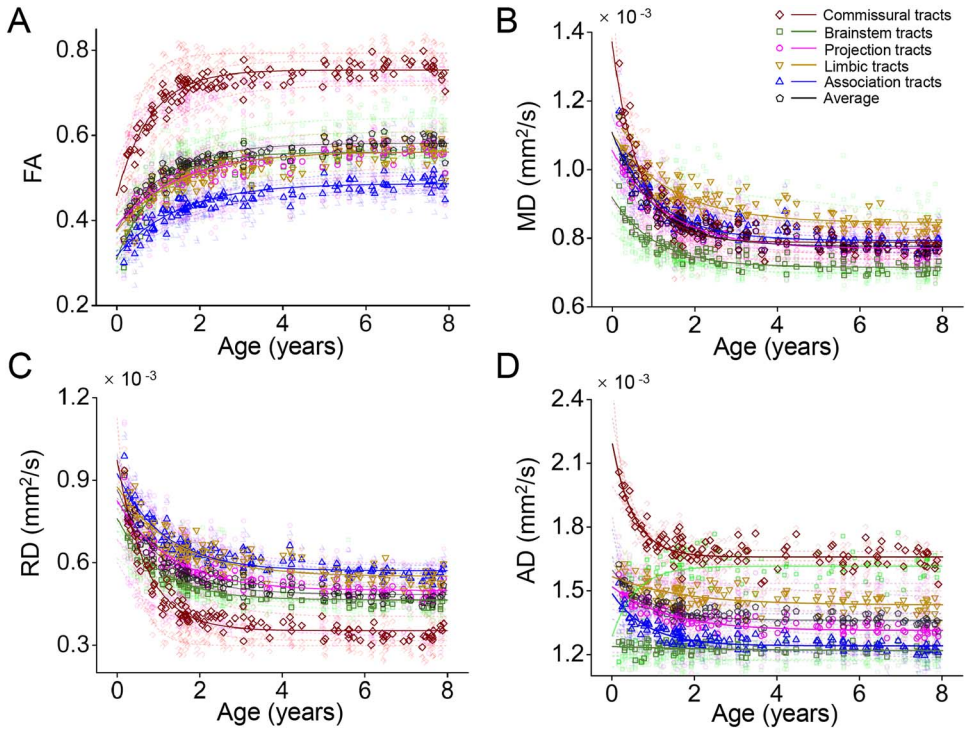

Figure 3. Differential microstructural maturational curve across all major WM tracts and tract groups measured with FA (*A*), MD (*B*), RD (*C*), and AD (*D*) measurements. Fitted exponential curves are shown for all tracts and tract groups. The fitted curves of DTI metric measurements averaged from the tract group were plotted in solid line and those from individual WM tracts were plotted in semitransparent dashed lines in the same color.

across WM tract groups are elaborated in the Supplemental Information.

DTI Acquisition and Measurement of Tract-Specific and Tract-Group-Specific WM Microstructure

All participants were scanned on a 3T Philips Achieva system (Philips, Best, the Netherlands) with sedation. DTI images were acquired using a single-shot EPI sequence with sensitivity encoding parallel imaging scheme (SENSE, reduction factor = 2). Earplug and headphones were used to minimize noise exposure. The imaging matrix size was 128×128 with a field of view of 256×256 mm^2. Axial slices with 2 mm thickness were acquired parallel to the anterior-posterior commissure line. A total of 70 slices covered the entire brain without the gap. The repetition time and echo time were 9.3 s and 100 ms, respectively. Diffusion weighting was encoded along 30 independent directions (Jones et al. 1999), and the b-value was 1000 sec/mm^2. To improve the signal-to-noise ratio, two repetitions were performed. Visual inspection was conducted for all DTI data by the pediatric radiologists (H.K. and Y.P.) and no apparent motion artifacts were caught. Automated image registration from DTIStudio (Jiang et al. 2006) was applied to raw diffusion weighted images to correct distortion caused by eddy current. Head motions in DTI data were quantified for all subjects. As shown in Supplementary Figure S1, few motion artifacts were observed in both TD and ASD subjects with less than 0.5 mm in translation and less than 0.25 degrees in rotation for all subjects. There are no significant differences in translation ($P = 0.41$) and rotation ($P = 0.06$) between ASD and TD groups, either. The standard tensor fitting was conducted with DTIStudio to generate whole-brain maps of four DTI-derived metrics: FA, MD, RD, and AD. The atlas-based labeling of WM skeleton is as follows. Briefly, after nonlinear registration to a single-subject template used in digital WM atlas (JHU ICBM-DTI-81) (Mori et al. 2008), all the FA images of 118 TD children and 31 ASD children were averaged in this template space. The skeleton of the group-averaged FA map was generated with tract-based spatial statistics (TBSS) (Smith et al. 2006) of FSL software (https://fsl.fmrib.ox.ac.uk/fsl/fslwiki/TBSS/) to extract the core of the WM tracts and alleviate partial volume effects, similar to the procedures described in detail in our previous publications (Huang et al. 2011, 2012). To minimize spurious voxels caused by noise, the threshold of the FA skeleton was set to 0.2 (Smith et al. 2006) with the resultant WM skeleton shown in Figure 1A. After the labels of each WM tract from the JHU ICBM-DTI-81 atlas (Mori et al. 2008) were transferred to the WM skeleton in the template space, each WM skeleton voxel was categorized into one tract and one tract group (Fig. 1B) (Wakana et al. 2004). The labeled and skeletonized WM tract groups are described as follows: 1) commissural tracts, including splenium (SCC), body (BCC), and genu (GCC) corpus callosum; 2) brainstem tracts, including inferior (ICP), middle (MCP), and superior (SCP) cerebellar peduncles, pontine crossing tract (PCT), and medial lemniscus (ML); 3) projection tracts, including corticospinal tract (CST), cerebral peduncle (CP), internal capsule (subdivided into anterior (AIC), posterior (PIC), and retrolenticular (RIC) portions), and corona radiata (subdivided into anterior (ACR), superior (SCR), and posterior (PCR) portions); 4) limbic tracts, including cingulum (subdivided into cingulate (CGC) and hippocampal (CGH) portions), and fornix (FX); and 5) association tracts

Table 1 The percent change (%) of DTI measurements (FA, MD, RD, and AD) from 0 to 8 years for each tract and tract group. "—" indicates measurements not available or with nonsignificant exponential fitting. The percent change of DTI measurements in this table was encoded as color shown on the left panel of Figures 5–8

	FA	MD	RD	AD
ALL	54.4	−29.9	−44.1	−14.7
Commissural	64.8	−42.5	−63.8	−24.2
SCC	92.1	−53	−73.6	−34.6
GCC	54.2	−45.1	−65.9	−29
BCC	71.2	−37.4	−59.5	−15.3
Brainstem	81.9	−22.1	−39	—
PCT	104	−18.8	−38.9	—
MCP	90.1	−26.6	−42.2	−6.9
ICP	69	−20.3	−35.8	—
SCP	59	—	−28.9	25.7
ML	48.5	−12.3	−30.1	8
Association	54	−28.3	−38.2	−16.4
SLF	63.8	−32.7	−42.9	−19.6
SFOF	71.8	−22.2	−34	−8.1
UF	59.4	−22.6	−37.8	—
EC	41.8	−21.9	−30.9	−11.3
SS	57.5	−30.3	−40.3	−24.2
Limbic	49.9	−23.5	−37.1	−8.4
FX	44.7	−24	−38.7	−9.4
CGC	62.2	−28.2	−42.5	−11.1
CGH	40.6	−17.4	−29.5	—
Projection	44.7	−27	−39.5	−13.5
PIC	35.8	−20	−41.9	−6.2
RIC	35.3	−23.1	−34.9	−11.8
AIC	57.1	−22.2	−38.3	−5.2
PCR	51.6	−28.2	−37.8	−16.4
CP	43.8	−28	−51.6	−16.8
SCR	46.6	−29.5	−39.1	−18.3
ACR	56.5	−31.5	−41	−19.6
CST	43.6	−21.3	−33	—

(corticocortical tracts connecting two cortical regions), including external capsule (EC), superior fronto-occipital fasciculus (SFOF), superior longitudinal fasciculus (SLF), sagittal stratum (SS), and uncinate fasciculus (UF). The tract-specific or tract-group-specific FA, MD, RD, and AD of all major 24 WM tracts and 5 tract groups were then obtained by averaging these measurements with these labeled WM skeletons as the regions-of-interest (Fig. 1C). The FA, MD, RD, or AD differences among major WM tracts or tract groups within the subjects were tested with ANOVA. The entire WM was used as a reference to examine the differential microstructural maturation of all tracts and tract groups.

Curve Fitting of FA, MD, RD, and AD of all Major WM Tracts and Tract Groups

As shown in Supplemental information, AIC was used to quantify the relative goodness-of-fit among different models (including linear, exponential, logarithmic, Poisson, and quadratic polynomial) for fitting the microstructural maturational curves of the entire WM of TD children. Among the five models, the highest coefficient of determination (R^2) in FA (R^2 = 89.6%), MD (R^2 = 89.5%), RD (R^2 = 90.4%), and AD (R^2 = 76.8%) was found with exponential model $f(x) = a \cdot e^{-bx} + c$ (Fig. S2 and Table S1). The exponential model $f(x) = a \cdot e^{-bx} + c$ was then used to fit the maturational curve of WM microstructure of all WM tracts and tract groups, with x the age of the subject and $f(x)$ the tract-specific or tract-group-specific DTI measurements (e.g., FA, MD, RD, or AD). All fitted parameters b and c were positive. Fitted parameter a was negative or positive when the DTI measurements increased or decreased with age. After fitting all major WM tracts and tract groups with the exponential model, the percent change of each DTI metric was also quantified based on the fitting curve. For example, the FA percentage change in the fitted exponential curve was defined as ($F\hat{A}$ (age = 8 years)—$F\hat{A}$ (age = 0 year))/$F\hat{A}$ (age = 0 year), with $F\hat{A}$ representing the FA value in the fitted exponential curve. Furthermore, the two time points *t1* and *t2* when the ($F\hat{A}$ (t)—$F\hat{A}$ (age = 0 year)) value reaches the 2/3 and 8/9 of the ($F\hat{A}$ (age = 8 years)—$F\hat{A}$ (age = 0 year)) value in each fitted exponential curve were identified. The fitted exponential curve of each tract or tract group was divided into three phases, namely *fast*, *intermediate*, and *slow* phase, with these two time points separating the curve in 0–8 years. Similar procedures were applied to fitted MD, RD, and AD curves.

Each fitted exponential line was modulated by three parameters (a, b, and c) that play important roles to characterize differentiated WM microstructural maturational curve $f(x) = a \cdot e^{-bx} + c$. As shown in Figure S3, a larger absolute value of the parameter a (abs(a)) indicates a larger increase (or decrease) of the DTI measurement from $f(0)$ to $f(x)$. A larger b indicates a steeper increase in the earlier phase of the developmental curve. A larger c indicates the overall elevation of the developmental curve. The difference of each parameter of a certain tract or tract group

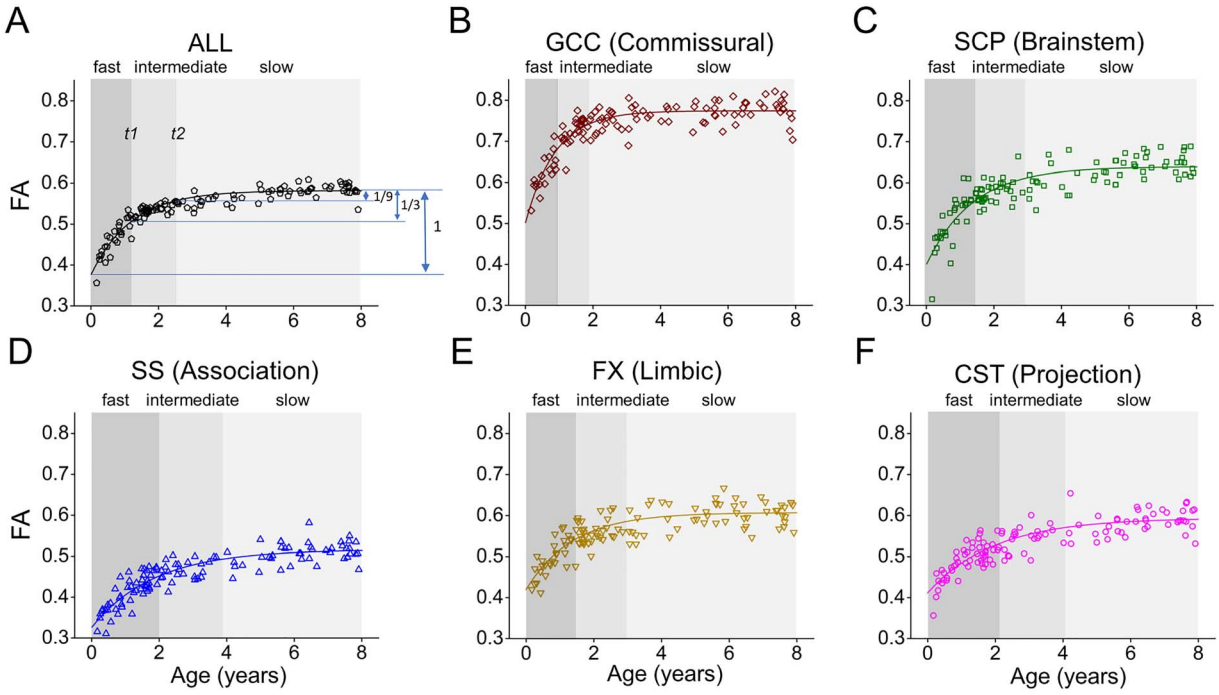

Figure 4. Three phases (*fast*, *intermediate*, and *slow* phases) identified from fitted exponential maturational FA curve of the averaged entire WM (*A*) and a representative tract, namely GCC (*B*), SCP (*C*), SS (*D*), FX (*E*), and CST(*F*), from each of five tract groups. The ages *t1* and *t2* when the (FÂ(t)—FÂ (age = 0 year)) value reaches the 2/3 and 8/9 of the (FÂ(age = 8 years)—FÂ (age = 0 year)) value in each fitted exponential curve were used to separate the WM maturation into three phases: *fast*, *intermediate*, and *slow* phases. Please see the Materials and Methods section for abbreviations of WM tract names.

and that of the entire WM was tested with permutation tests with details in Supplemental Information. Differences between left and right tracts were also tested with permutation tests to evaluate the asymmetry of WM microstructural maturation.

Results

Overview of WM Microstructural Profile Characterized by DTI-Derived FA, MD, RD, AD, and Orientation-Encoded Colormap

All abbreviations of WM tracts can be found in the legend of Figure 1. Figure 2A shows the DTI-derived metric maps, including FA, MD, RD, AD and orientation-encoded colormap (OEC) maps, of representative TD brains at 2, 13, 24, 48, and 95 months. As shown in Supplemental Information, the microstructural properties among WM tracts and tract groups are heterogenous within the subjects, regardless of the ages. Very dynamic brain WM changes from birth to 8 years of age can be appreciated from Figure 2A, characterized by prominent FA increases and prominent RD and MD decreases. Axonal maturational processes including axonal growth, axional packing, and myelination may contribute to these DTI-derived metric changes, according to the DTI signal model (Beaulieu 2002; Song et al. 2003; Haynes et al. 2005; Dubois et al. 2006, 2008; Lebel et al. 2008; Gao et al. 2009) illustrated in Figure 2B.

Three Phases in the WM Tract Maturational Curve

The age-related changes of FA, MD, RD, and AD, fitted with exponential model, of all WM tracts are shown in Figure 3. The percent changes of all tracts with FA, MD, RD, and AD measurements are listed in Table 1. In the FA maturational curves of 0–8 years of the WM tracts GCC, SCP, SS, FX, and CST shown in Figure 4, the FA increases rapidly at the beginning in the *fast* phase, then slows down in the *intermediate* phase, and at last reaches the *slow* phase with mild increase. GCC, SCP, SS, FX, and CST are representative tract in each of five WM tract groups, respectively. The WM tract with shorter *fast* and *intermediate* phases matures earlier. For example, the end of *fast* and *intermediate* phases (*t1* and *t2*) of GCC at 0.97 years and 1.94 years is much earlier than the corresponding timings of SCP (1.49 and 2.96 years), SS (1.98 and 3.87 years), FX (1.5 and 2.99 years), and CST (2.1 and 4.08 years), suggesting that the GCC matures earlier than other four tracts. The WM developments within the three WM maturational phases are all linear across all tracts and tract groups (all $P > 0.05$ for Kolmogorov–Smirnov test of residual). The three phases measured in FA, MD, RD, and AD are listed in Tables 2.–5., respectively.

Differential Maturation of WM Tracts and Tract Groups

The differential maturational curves based on FA, MD, RD, and AD measurements are represented by the percent change, timing of three phases (left panel of Figs 5–8), and key exponential fitting parameters (right panel of Figs 5–8). As shown on the left panel of Figure 5, with the percentage increase of the entire WM FA 54.4%, larger FA percent increases (warmer colors in the horizontal bars) of the commissural (64.8%) and brainstem (81.9%) tract groups and smaller FA percent increases (colder colors in the horizontal bars) of the limbic (49.9%), projection (44.7%), and association (54%) tract groups were observed. Also shown in the left panel of Figure 5 and Table 2., earlier

Table 2 The start and end age (years) as well as duration (years) of each phase for each tract and tract group in FA, ordered by the length of the fast phase. Please see the Materials and Methods section for abbreviations of WM tract names

	Fast		*Intermediate*		*Slow*	
	0–t1	Length	t1–t2	Length	t2–	Length
All	0–1.3	1.3	1.3–2.6	1.3	2.6–	—
Commissural	0–0.9	0.9	0.9–1.79	0.9	1.79–	—
Brainstem	0–1.08	1.08	1.08–2.15	1.07	2.15–	—
Association	0–1.61	1.61	1.16–3.19	1.58	3.19–	—
Limbic	0–1.63	1.63	1.63–3.23	1.6	3.23–	—
Projection	0–1.64	1.64	1.64–3.25	1.61	3.25–	—
SCC	0–0.49	0.49	0.49–0.97	0.49	0.97–	—
PCT	0–0.87	0.87	0.87–1.74	0.87	1.74–	—
PIC	0–0.87	0.87	0.87–1.74	0.87	1.74–	—
GCC	0–0.97	0.97	0.97–1.94	0.97	1.94–	—
MCP	0–1.03	1.03	1.03–2.06	1.03	2.06–	—
ICP	0–1.17	1.17	1.17–2.33	1.16	2.33–	—
BCC	0–1.19	1.19	1.19–2.37	1.18	2.37–	—
RIC	0–1.2	1.2	1.2–2.39	1.19	2.39–	—
AIC	0–1.31	1.31	1.31–2.61	1.3	2.61–	—
SLF	0–1.34	1.34	1.34–2.68	1.34	2.68–	—
SCP	0–1.49	1.49	1.49–2.96	1.47	2.96–	—
FX	0–1.5	1.5	1.5–2.99	1.49	2.99–	—
CGC	0–1.55	1.55	1.55–3.07	1.53	3.07–	—
PCR	0–1.58	1.58	1.58–3.14	1.56	3.14–	—
ML	0–1.67	1.67	1.67–3.31	1.64	3.31–	—
SFOF	0–1.72	1.72	1.72–3.41	1.68	3.41–	—
UF	0–1.73	1.73	1.73–3.43	1.69	3.43–	—
CP	0–1.8	1.8	1.8–3.55	1.75	3.55–	—
CGH	0–1.83	1.83	1.83–3.6	1.77	3.6–	—
EC	0–1.83	1.83	1.83–3.6	1.77	3.6–	—
SCR	0–1.96	1.96	1.96–3.83	1.87	3.83–	—
SS	0–1.98	1.98	1.98–3.87	1.89	3.87–	—
ACR	0–2.03	2.03	2. 03–3.96	1.93	3.96–	—
CST	0–2.1	2.1	2.1–4.08	1.98	4.08–	—

end ages of *fast* and *intermediate* phases of the commissural (0.9 and 1.79 years) and brainstem (1.08 and 2.15 years) tract groups and later corresponding timings for the limbic (1.63 and 3.23 years), projection (1.64 and 3.25 years), and association (1.61 and 3.19 years) tract groups were observed, compared with those of the entire WM (1.3 and 2.6 years). Consistent with observed phases in FA measurements, the earlier end ages of fast and intermediate phases were also found in commissural tract groups with MD (0.72 and 1.44 years), RD (0.78 and 1.57 years), and AD (0.56 and 1.13 years) measurements, and later corresponding ages for the limbic (MD: 1.57 and 3.12 years, RD: 1.53 and 3.05 years, AD: 1.81 and 3.56 years), projection (MD: 1.42 and 2.84 years, RD: 1.41 and 2.81 years, AD: 1.46 and 2.92 years), and association (MD: 1.17 and 2.34 years, RD: 1.24 and 2.48 years, AD: 0.94 and 1.87 years) tract groups (Tables 3.–5.) were observed.

The parameters *a*, *b*, and *c* of fitted exponential curves of FA measurements of all tracts are presented on the right panel of Figure 5. Significant differences in the parameter *a*, *b*, or *c* between a specific tract/tract group and entire WM indicates differentiated WM maturation (Fig. 5). For example, significantly higher abs(*a*), *b,* and *c* values of commissural tracts than those of entire WM indicate significantly larger magnitude of age-related increase, steeper increase for earlier phase, and bigger overall elevation, respectively (Fig. S3).

As shown in Figure S6, significant difference of fitted *a* or *b* parameter between left and right tracts was not found for most of the tracts. Significant differences of fitted *c* parameter between left and right tract were shown for a few tracts. Of note, the parameter *c* of left SLF and CGC from FA measurement is higher than that of the corresponding right tract, suggesting higher microstructural integrity of SLF and CGC in the left hemisphere.

Larger Microstructural Residual Variance in the WM of Children with ASD During Brain Development from 2 to 8 Years of Age

Larger residual variances of WM maturation of children with ASD compared with TD children were found broadly across WM tract groups, as shown in Figures S4 and S5.

Discussion

In this study, we found differential and significant microstructural changes with DTI-derived metric measurements of all major WM tracts and tract groups from a relatively large sample size of children ($n = 118$) from 0 to 8 years of age. The maturational curve of the entire WM microstructure was best fitted with an exponential model. The WM microstructural maturational process of each tract or tract group was char-

Table 3 The start and end age (years) as well as duration (years) of each phase for each tract and tract group in MD, ordered by the length of the *fast* phase. Please see the Materials and Methods section for abbreviations of WM tract names. "—" indicates measurements not available or with nonsignificant exponential fitting

	Fast		*Intermediate*		*Slow*	
	0–t1	Length	t1–t2	Length	t2–	Length
ALL	0–1.09	1.09	1.09–2.19	1.09	2.19–	—
Commissural	0–0.72	0.72	0.72–1.44	0.72	1.44–	—
Brainstem	0–1.15	1.15	1.15–2.31	1.15	2.31–	—
Association	0–1.17	1.17	1.17–2.34	1.17	2.34–	—
Projection	0–1.42	1.42	1.42–2.84	1.41	2.84–	—
Limbic	0–1.57	1.57	1.57–3.12	1.55	3.12–	—
SCC	0–0.39	0.39	0.39–0.79	0.39	0.79–	—
GCC	0–0.73	0.73	0.73–1.47	0.73	1.47–	—
CST	0–0.97	0.97	0.97–1.93	0.96	1.93–	—
PCT	0–1.02	1.02	1.02–2.03	1.02	2.03–	—
MCP	0–1.02	1.02	1.02–2.04	1.02	2.04–	—
SS	0–1.05	1.05	1.05–2.09	1.04	2.09–	—
BCC	0–1.05	1.05	1.05–2.1	1.05	2.1–	—
ML	0–1.07	1.07	1.07–2.14	1.07	2.14–	—
SLF	0–1.09	1.09	1.09–2.18	1.09	2.18–	—
ICP	0–1.11	1.11	1.11–2.22	1.11	2.22–	—
CP	0–1.17	1.17	1.17–2.33	1.16	2.33–	—
EC	0–1.35	1.35	1.35–2.69	1.34	2.69–	—
FX	0–1.36	1.36	1.36–2.71	1.35	2.71–	—
AIC	0–1.36	1.36	1.36–2.71	1.35	2.71–	—
PIC	0–1.36	1.36	1.36–2.71	1.35	2.71–	—
CGC	0–1.4	1.4	1.4–2.78	1.39	2.78–	—
UF	0–1.4	1.4	1.4–2.79	1.39	2.79–	—
SCR	0–1.45	1.45	1.45–2.89	1.44	2.89–	—
RIC	0–1.45	1.45	1.45–2.89	1.44	2.89–	—
PCR	0–1.48	1.48	1.48–2.94	1.46	2.94–	—
ACR	0–1.52	1.52	1.52–3.01	1.5	3.01–	—
CGH	0–1.8	1.8	1.8–3.55	1.75	3.55–	—
SFOF	0–2.36	2.36	2.36–4.51	2.14	4.51–	—
SCP	—	—	—	—	—	—

acterized by three distinct phases, *fast*, *intermediate,* and *slow* phases from 0 to 8 years, based on the fitted exponential curve. The start and end age as well as the duration of each phase have been charted for each tract and tract group. Furthermore, we found that microstructural maturational processes were differential among tracts and tract groups by comparing the corresponding parameters of maturational curves of these tracts or tract groups. With quantified information of TD WM development, larger residual variance of WM maturation in ASD children was found, suggesting that the established normal WM trajectories and tables could be used as a reference for delineating altered maturation of children with neuropsychiatric disorders.

The DTI data presented in this study were scanned with uniform imaging parameters on an identical 3T MR system, making it possible to explore the differential WM maturational pattern that could not be well appreciated with isolated and fragmented age ranges. The results unified the linear (Dubois et al. 2006; Schmithorst et al. 2008; Asato et al. 2010) and nonlinear (Mukherjee et al. 2001; Schneider et al. 2004; Lebel et al. 2008, 2012; Westlye et al. 2010; Lebel and Beaulieu 2011; Deoni et al. 2012; Sadeghi et al. 2013; Yu et al. 2014) findings of WM maturation from previous studies. Only with the relatively large age range presented in this study, does it become clear that linear model is no longer valid for characterizing the WM developmental pattern, as the developmental rates are quite different among these different phases. Besides providing good coverage of critical developmental stages, the relatively large sample size used in this study could enable certain conclusions with statistical significance. Spatiotemporal heterogeneity of WM maturation might be only appreciated with larger age range and sufficient sample size. To our knowledge, this study quantitatively charted the three distinct developmental stages observed and maturational curves of all major WM tracts and tract groups from 0 to 8 years for the first time. These quantitative measurements of the differential stages of WM microstructural maturation based on DTI measurements could be an invaluable public resource as a reference for normal development to detect pediatric neuropsychiatric or neurological disorders. All WM maturational charts and DTI metric measurements can be freely downloaded from brainmrimap.org.

Possible Biological Processes Underlying WM Maturation from 0 to 8 Years

Previous histological studies have suggested that developmental processes such as myelination, axonal growth, and axonal packing occur in a differential manner across the brain WM regions during various maturational periods (Brody et al. 1987; Kinney et al. 1988; Hasegawa et al. 1992; Haynes et al. 2005; Clowry et al.

Table 4 The start and end age (years) as well as duration (years) of each phase for each tract and tract group in RD, ordered by the length of the *fast* phase. Please see the Materials and Methods section for abbreviations of WM tract names

	Fast		*Intermediate*		*Slow*	
	0–t1	Length	t1–t2	Length	t2–	Length
ALL	0–1.13	1.13	1.13–2.26	1.13	2.26–	—
Commissural	0–0.78	0.78	0.78–1.57	0.78	1.57–	—
Brainstem	0–1.13	1.13	1.13–2.25	1.12	2.25–	—
Association	0–1.24	1.24	1.24–2.48	1.24	2.48–	—
Projection	0–1.41	1.41	1.41–2.81	1.4	2.81–	—
Limbic	0–1.53	1.53	1.53–3.05	1.52	3.05–	—
SCC	0–0.42	0.42	0.42–0.84	0.42	0.84–	—
GCC	0–0.81	0.81	0.81–1.62	0.81	1.62–	—
PCT	0–0.91	0.91	0.91–1.82	0.91	1.82–	—
PIC	0–0.98	0.98	0.98–1.96	0.98	1.96–	—
MCP	0–1.02	1.02	1.02–2.03	1.01	2.03–	—
BCC	0–1.07	1.07	1.07–2.13	1.07	2.13–	—
SLF	0–1.1	1.1	1.1–2.21	1.1	2.21–	—
ICP	0–1.2	1.2	1.2–2.4	1.2	2.4–	—
RIC	0–1.26	1.26	1.26–2.52	1.26	2.52–	—
AIC	0–1.27	1.27	1.27–2.54	1.27	2.54–	—
SS	0–1.29	1.29	1.29–2.57	1.28	2.57–	—
CGC	0–1.36	1.36	1.36–2.72	1.35	2.72–	—
FX	0–1.4	1.4	1.4–2.79	1.39	2.79–	—
PCR	0–1.41	1.41	1.41–2.81	1.4	2.81–	—
EC	0–1.42	1.42	1.42–2.84	1.41	2.84–	—
SCR	0–1.48	1.48	1.48–2.94	1.46	2.94–	—
ML	0–1.48	1.48	1.48–2.95	1.47	2.95–	—
UF	0–1.5	1.5	1.5–2.99	1.49	2.99–	—
CP	0–1.5	1.5	1.5–2.99	1.49	2.99–	—
ACR	0–1.55	1.55	1.55–3.08	1.53	3.08–	—
CST	0–1.55	1.55	1.55–3.09	1.53	3.09–	—
CGH	0–1.68	1.68	1.68–3.32	1.64	3.32–	—
SFOF	0–2.04	2.04	2.04–3.98	1.94	3.98–	—
SCP	0–3.32	3.32	3.32–5.74	2.42	5.74–	—

2010). Certain relationship between DTI metric measurements and cellular processes in WM development (Beaulieu 2002; Song et al. 2003; Haynes et al. 2005; Dubois et al. 2006, 2008; Lebel et al. 2008; Gao et al. 2009) was inferred in Figure 2B. Specifically, axonal growth in fascicles is associated with an increase of AD, and also with increases of FA and MD. Axonal packing is associated with decrease of AD and RD, leading to an increase of FA and a decrease of MD. WM myelination is associated with a decrease of RD, resulting in an increase of FA and a decrease of MD. As shown in Figure 3, myelination and axonal packing might play a signficant role for WM maturation in 0–8 years with increased FA, decreased MD, and decreased RD (Brody et al. 1987; Kinney et al. 1988; Song et al. 2002; Hermoye et al. 2006; Geng et al. 2012). Commissural and association tract groups might be associated with the highest and lowest myelination/axonal packing level, respectively, in the studied age range.

Three Characteristic Developmental Phases from 0 to 8 Years

The exponential model fitted the WM maturational data better than linear, polynomial, Poisson, and logarithmic models (Fig. S2 & Table S1). With significantly fitted exponential curves for all major tracts and tract groups with FA and RD measurements and for most of tracts and tract groups with MD and AD measurements, three characteristic developmental phases were defined (Figs 4–8, Tables 2.–5.). Specifically, these three phases are *fast*, *intermediate*, and *slow* phases with the *fast* phase usually occurring in infancy (ending between 0.49 and 2.1 years according to FA measurements), the *slow* phase lasting longest, and the *intermediate* phase presenting as a transitional phase between the *fast* and *slow* phases; 1/3 and 1/9 were arbitrarily chosen (Fig. 4) to make the logarithm of FA(t), MD(t), RD(t), or AD(t) evenly divided by log(1/3) with exponential function modeled for these DTI measurements. Consistent with previous studies (Brody et al. 1987; Hermoye et al. 2006; Geng et al. 2012; Simmonds et al. 2014), FA measurements of the commissural tracts reach the *slow* phase earliest among all WM tracts as the FA measurements of commissural tracts demonstrate the fastest increase in *fast* phase. Accordingly, the *slow* phase of the FA measurements of commissural tracts is the longest (Figs 4B and 5 and Table 2.). On the other hand, FA values of the CST undergo steady and continuous increase from 0–8 years (Fig. 4F) with the duration of the *slow* phase before 8 years the shortest of all WM tracts. This is consistent with the prolonged myelination of CST until adolescence (Lebel et al. 2008; Lebel and Beaulieu 2011).

Table 5 The start and end age (years) as well as duration (years) of each phase for each tract and tract group in AD, ordered by the length of the *fast* phase. Please see the Materials and Methods section for abbreviations of WM tract names. "—" indicates measurements not available or with nonsignificant exponential fitting

	Fast		*Intermediate*		*Slow*	
	0–t1	Length	t1–t2	Length	t2–	Length
ALL	0–0.97	0.97	0.97–1.94	0.97	1.94–	—
Commissural	0–0.56	0.56	0.56–1.13	0.56	1.13–	—
Association	0–0.94	0.94	0.94–1.87	0.94	1.87–	—
Projection	0–1.46	1.46	1.46–2.92	1.45	2.92–	—
Limbic	0–1.81	1.81	1.81–3.56	1.75	3.56–	—
Brainstem	—	—	—	—	—	—
CP	0–0.27	0.27	0.27–0.55	0.27	0.55–	—
UF	—	—	—	—	—	—
SCC	0–0.35	0.35	0.35–0.69	0.35	0.69–	—
SS	0–0.43	0.43	0.43–0.87	0.43	0.87–	—
ICP	—	—	—	—	—	—
GCC	0–0.6	0.6	0.6–1.19	0.6	1.19–	—
SCP	0–0.62	0.62	0.62–1.23	0.62	1.23–	—
PCT	—	—	—	—	—	—
BCC	0–0.98	0.98	0.98–1.96	0.98	1.96–	—
SLF	0–1.04	1.04	1.04–2.08	1.04	2.08–	—
MCP	0–1.04	1.04	1.04–2.09	1.04	2.09–	—
EC	0–1.08	1.08	1.08–2.17	1.08	2.17–	—
FX	0–1.11	1.11	1.11–2.21	1.1	2.21–	—
SCR	0–1.39	1.39	1.39–2.77	1.38	2.77–	—
ACR	0–1.43	1.43	1.43–2.84	1.42	2.84–	—
CGC	0–1.58	1.58	1.58–3.13	1.55	3.13–	—
PCR	0–1.68	1.68	1.68–3.33	1.65	3.33–	—
RIC	0–1.99	1.99	1.99–3.89	1.9	3.89–	—
AIC	0–2.23	2.23	2.23–4.29	2.06	4.29–	—
ML	0–2.63	2.63	2.63–4.91	2.27	4.91–	—
SFOF	0–4.13	4.13	4.13–6.43	2.31	6.43–	—
PIC	0–4.47	4.47	4.47–6.66	2.19	6.66–	—
CGH	—	—	—	—	—	—
CST	—	—	—	—	—	—

Differentiated Maturation Across WM Tracts and WM Tract Groups

Despite the previous reports of differentiated maturation among WM tracts (Geng et al. 2012; Kersbergen et al. 2014; Yu et al. 2016; Ouyang et al. 2019a) with DTI measurements, the maturational curves of the tracts have not been systematically and quantitatively compared with appropriate modeling. The differential WM maturation pattern was revealed by the comparison of the three fitting parameters among WM tracts and tract groups (Figs 5–8). The directional changes of the parameters of the commissural tract group (FA: abs(a)↑, b↑, c↑; RD: a↑, b↑, c↓; AD: a↑, b↑, c↑) compared with the average of the entire WM suggest that the commissural tracts are characterized with 1) a higher level of axonal growth (AD: c↑) and myelination (FA: c↑; RD: c↓); 2) a larger overall increase of axonal packing (AD: a↑) and myelination (FA: abs(a)↑; RD: a↑); and 3) earlier axonal packing (AD: b↑) and myelination (FA: b↑; RD: b↑). On the contrary, the parameter changes of the projection tract group (FA: abs(a)↓, b↓, c↓; RD: a↓, b↓, c↑; AD: a↓, b↓, c↓) suggest that the projection tracts are characterized with 1) a lower level of axonal growth (AD: c↓) and myelination (FA: c↓; RD: c↑); 2) smaller overall increase of axonal packing (AD: a↓) and myelination (FA: abs(a)↓; RD: a↓); and 3) later axonal packing (AD: b↓) and myelination (FA: b↓; RD: b↓). Consistent with maturational patterns of synaptic density, dendritic tree, and myelination from histological studies (Yakovlev and Lecours 1967; Kinney et al. 1988; Huttenlocher 1990; Rakic et al. 1994; Petanjek et al. 2008, 2011), two WM maturation patterns could be identified with the fitted parameters shown in Fig. 5: 1) WM develops from the posterior to anterior brain. For example, the SCC, PIC, and PCR mature earlier than the GCC, AIC, and ACR, respectively; 2) WM develops from the central to peripheral brain. For example, the commissural tract group matures earlier than the association tract group. The hierarchical maturation suggested by the results in this study is consistent with the brain developmental pattern from primary sensorimotor system to higher order functional system. The WM tracts connecting primary sensorimotor cortex, for example, SCC connecting to primary visual cortex, are among the earliest to develop in 0–8 years. Consistent with the protracted dendritic growth (e.g., Sedmak et al. 2018) and cognitive development (e.g., Rakic et al. 1994) till adolescence and adulthood, the microstructural changes of the corticocortical association WM tracts (e.g., SFOF and SLF) connecting to the prefrontal cortex are among the slowest to develop. From the perspective of WM microstructure, differential maturation of WM with early development of WM tracts involved in primary sensorimotor system (e.g., SCC connected to primary visual cortex) to protracted development of WM tracts involved in higher cognitive system (e.g., corticocortical association tracts

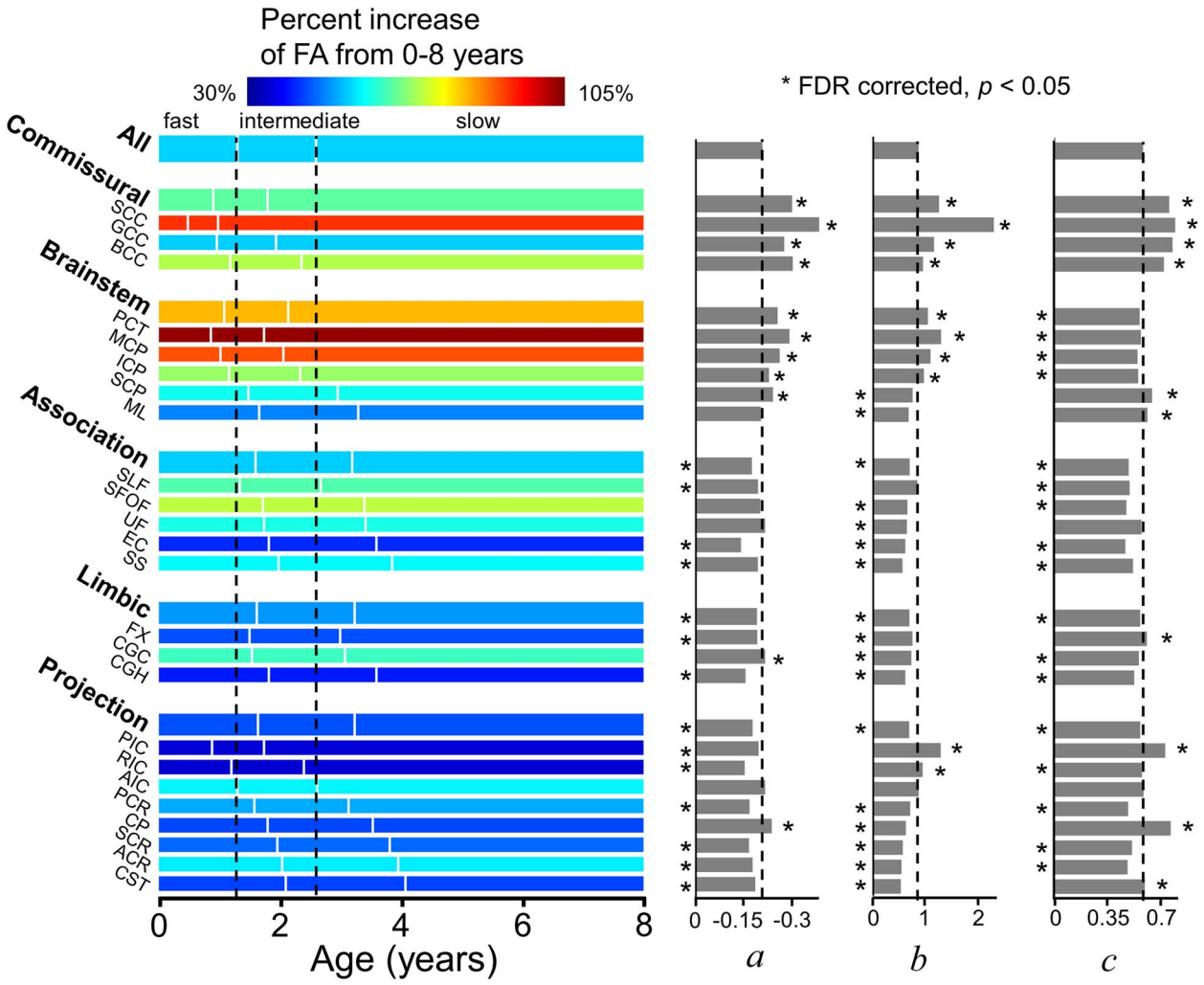

Figure 5. Illustration of percentage increase of FA from 0 to 8 years (with the percentage increase values listed in Table 1), three phases (with the start/end ages and phase length listed in Tables 2) and estimated fitting parameters *a*, *b*, *and c* of exponential curves of FA across all major WM tracts and tract groups. Measures of averaged entire WM were used as the reference. On the left panel, the WM maturation of every WM tract and tract group was displayed in three phases (*fast*, *intermediate*, and *slow* phases), with the boundaries of the three phases of the entire WM displayed as two reference dashed lines. The color bar encodes the percent increases of FA from 0 to 8 years. * indicates significant difference of a fitting parameter *a*, *b*, or *c* from that of the averaged entire WM, shown as black dashed lines. * placed on the left side indicates the abs(*a*), *b*, or *c* is significantly smaller than that of the entire WM's, and vice versa. Please see the Materials and Methods section for abbreviations of WM tract names.

connected to prefrontal cortex) sheds light on differential brain system development. Of note, DTI measurements are considered indirect compared with previous histological studies of WM maturation.

Application to ASD and Limitations of the Study

Alterations of WM microstructure have been observed within a plethora of neuropsychiatric disorders such as schizophrenia (Douaud et al. 2007), depression (Aghajani et al. 2014), bipolar disorder (Frazier et al. 2007), ASD (Barnea-Goraly et al. 2004), and ADHD (van Ewijk et al. 2014) in atypically developing brains. Established WM tract maturational curves of TD children could be used for early biomarker detection of the neuropsychiatric disorders showing group differences of DTI measurements from TD children, allowing for early intervention and precision health for infants and children. Hence, these TD WM maturational curves and charts have a potentially significant impact on health care of these mental disorders, with abnormal developmental process beginning years before the illness onset (Owen et al. 2011; Rapoport et al. 2012). Individuals with ASD are characterized by larger interindividual variability of both behavioral performance (Humphreys et al. 2007) and brain functional activity (Müller et al. 2003; Humphreys et al. 2008). With previous controversial findings of increasing (Bashat et al. 2007; Weinstein et al. 2011) and decreasing (Sundaram et al. 2008; Walker et al. 2012) WM microstructural integrity in children with ASD, WM microstructural residual variance of individuals with ASD was focused on. Larger intersubject variability of WM microstructure was found in several WM tract groups especially commissural tracts in children with ASD (Alexander et al. 2007), possibly underlying the larger

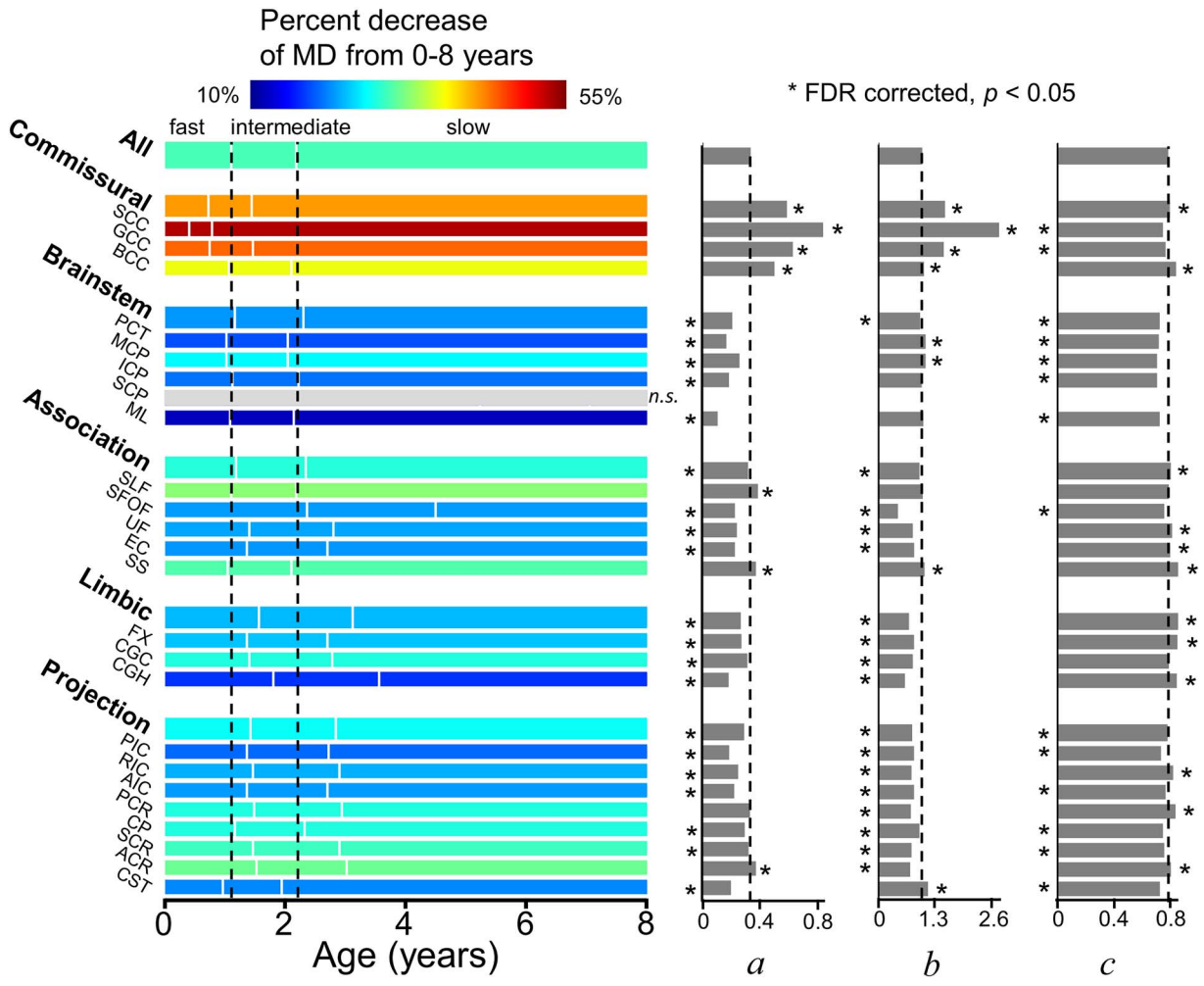

Figure 6. Illustration of percentage increase of MD from 0 to 8 years (with the percentage decrease values listed in Table 1), three phases (with the start/end ages and phase length listed in Table 3) and estimated fitting parameters *a*, *b*, and *c* of exponential curves of MD across all major WM tracts and tract groups. Measures of averaged entire WM were used as the reference. On the left panel, the WM maturation of every WM tract and tract group was displayed in three phases (fast, intermediate, and slow phases), with the boundaries of the three phases of the entire WM displayed as two reference dashed lines. The color bar encodes the percent decreases of MD from 0 to 8 years. * indicates significant difference of a fitting parameter *a*, *b*, or *c* from that of the averaged entire WM, shown as the black dashed lines. * placed on the left side indicates that the fitting parameter *a*, *b*, or *c* is significantly smaller than the entire WM's, and vice versa. With nonsignificant (n.s.) exponential fitting ($R^2 < 0.223$) of MD measurements of SCP, the percentage change of this specific tract is not available (shown in gray) and fitting parameters *a*, *b*, and *c* are not shown. Please see legend of Figure 1 for abbreviations of WM tract names.

interindividual behavioral variability of ASD (Humphreys et al. 2007; Turner and Stone 2007). Higher residual variances (Figs S4 and S5) of WM microstructure measured from children with ASD, compared with those of TD WM, are consistent with previous studies.

There are several limitations in this study. All presented data were cross-sectional. Delineating the individual longitudinal trajectory of WM maturation will build up an individual TD reference of WM microstructural maturation for precision medicine. A longitudinal study providing microstructural charts of WM tracts or tract groups is therefore warranted. A few other factors such as socioeconomic status could affect the WM microstructure, but were not accounted in this study. Compared with dramatic WM microstructural development during 0–8 years (e.g., FA percent change range 35–104%), the effects of other factors on charts of TD WM microstructural maturation would be relatively subtle. The tract-level and tract-group-level analysis could be further improved in the future with along-the-tract analysis (e.g., Mishra et al. 2015) and tract statistics (e.g., Goodlett et al. 2009). More complex models, such as diffusion kurtosis imaging (DKI) (Jensen et al. 2005) or neurite orientation dispersion and density imaging (NODDI) (Zhang et al. 2012), can bring extra WM microstructural information that cannot be characterized by DTI (see e.g., Ouyang et al. 2019b). With DTI-based metric measurements of WM tracts usually considered basis for more advanced diffusion models, the goal of this study was to fill the knowledge gap of DTI-based WM microstructural measurements for children aged 0–8 years. The DTI-based measurements of WM tracts in this study are very sensitive to capture the developmental changes, indicated by the low variance and high R^2 of the fitting. Further studies for testing sensitivity of advanced diffusion models and making charts with measurements of metrics from advanced models will extend the understanding of WM microstructural

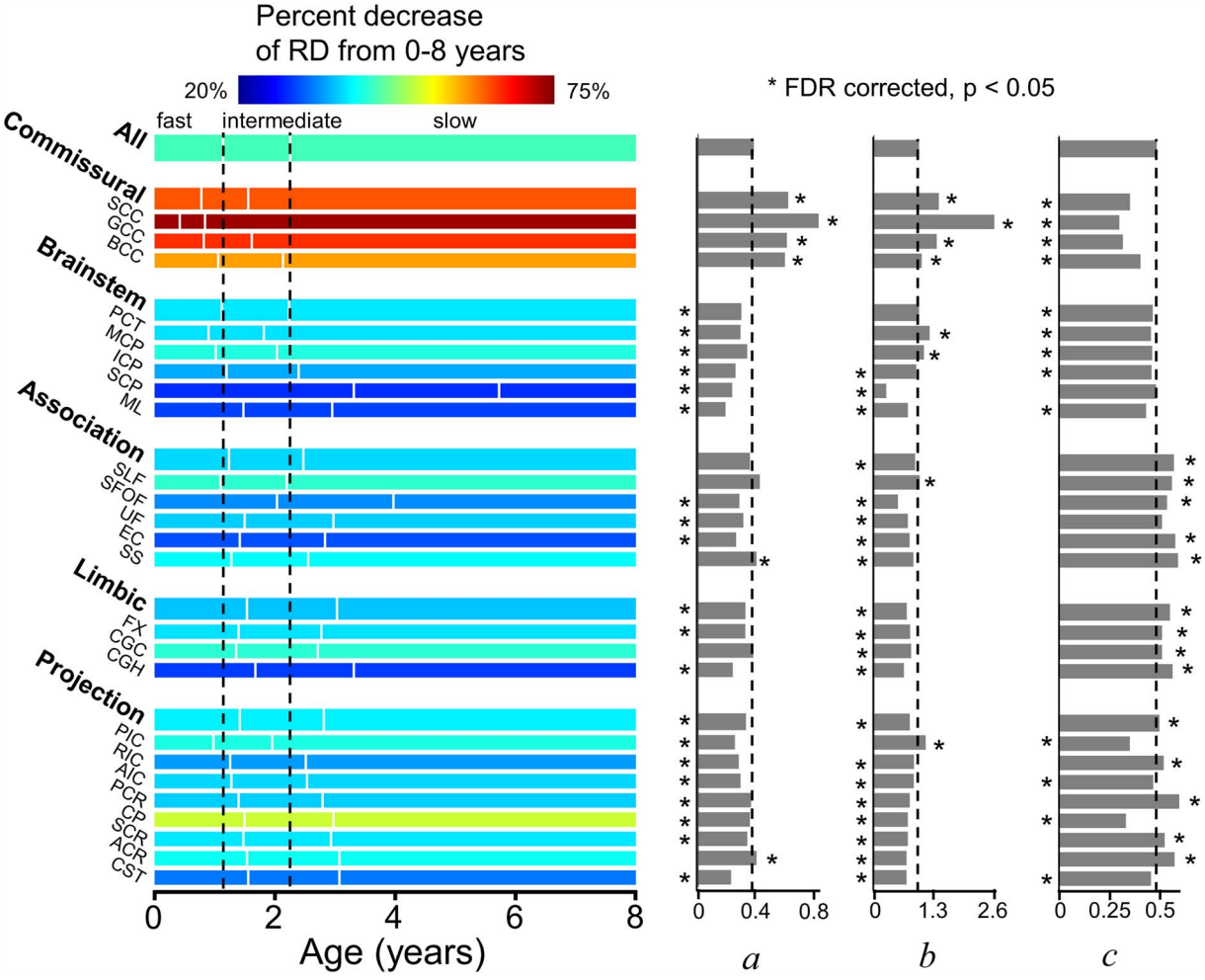

Figure 7. Illustration of percentage increase of RD from 0 to 8 years (with the percentage decrease values listed in Table 1), three phases (with the start/end ages and phase length listed in Table 4), and estimated fitting parameters *a*, *b*, and *c* of exponential curves of RD across all major WM tracts and tract groups. Measures of averaged entire WM were used as the reference. On the left panel, the WM maturation of every WM tract and tract group was displayed in three phases (fast, intermediate, and slow phases), with the boundaries of the three phases of the entire WM displayed as two reference dashed lines. The color bar encodes the percent decreases of RD from 0 to 8 years. * indicates significant difference of a fitting parameter *a*, *b*, or *c* from that of the averaged entire WM, shown as the black dashed lines. * placed on the left side indicates that the fitting parameter *a*, *b*, or *c* is significantly smaller than the entire WM's, and vice versa. Please see legend of Figure 1 for abbreviations of WM tract names.

maturation aged 0–8 years. As it was not practical to test all related maturation curve fitting models, the five candidate models tested in Figure S2 were among the most popular models used to fit WM maturation previously. The exponential model was optimal among those five models. It is possible that other curve fitting models (e.g., Gompertz function) could lead to better fitting than the exponential model.

Conclusion

We presented comprehensive and differential charts of TD WM microstructural maturation of all major tracts and tract groups in 0–8 years in the format of maturational curves and tables. The microstructural maturational curves of the entire WM were best fitted with the exponential model. The maturational curves were characterized by three phases and three critical fitting parameters, which are heterogeneous across the WM tracts or tract groups. The established charts were also used for detecting higher residual variances for children with ASD. Taken together, the maturational charts and tables covering all major WM tracts were established with DTI measurements of TD children aged 0–8 years, revealing early brain WM development pattern and offering reference standards for "pre" diagnostic risk assessment of neuropsychiatric disorders.

Supplementary Material

Supplementary material can be found at *Cerebral Cortex* online.

Funding

This work was supported in part by grants from the National Institute of Health to Dr Huang (NIHMH092535, MH092535-S1 and HD086984), the Chinese Ministry of Science and Technology to Dr Fang (MOST 2015CB351800), and the National Natural Science Foundation of China (NSFC) to Dr Fang (31421003 and 31671168) and Dr Peng (81671651).

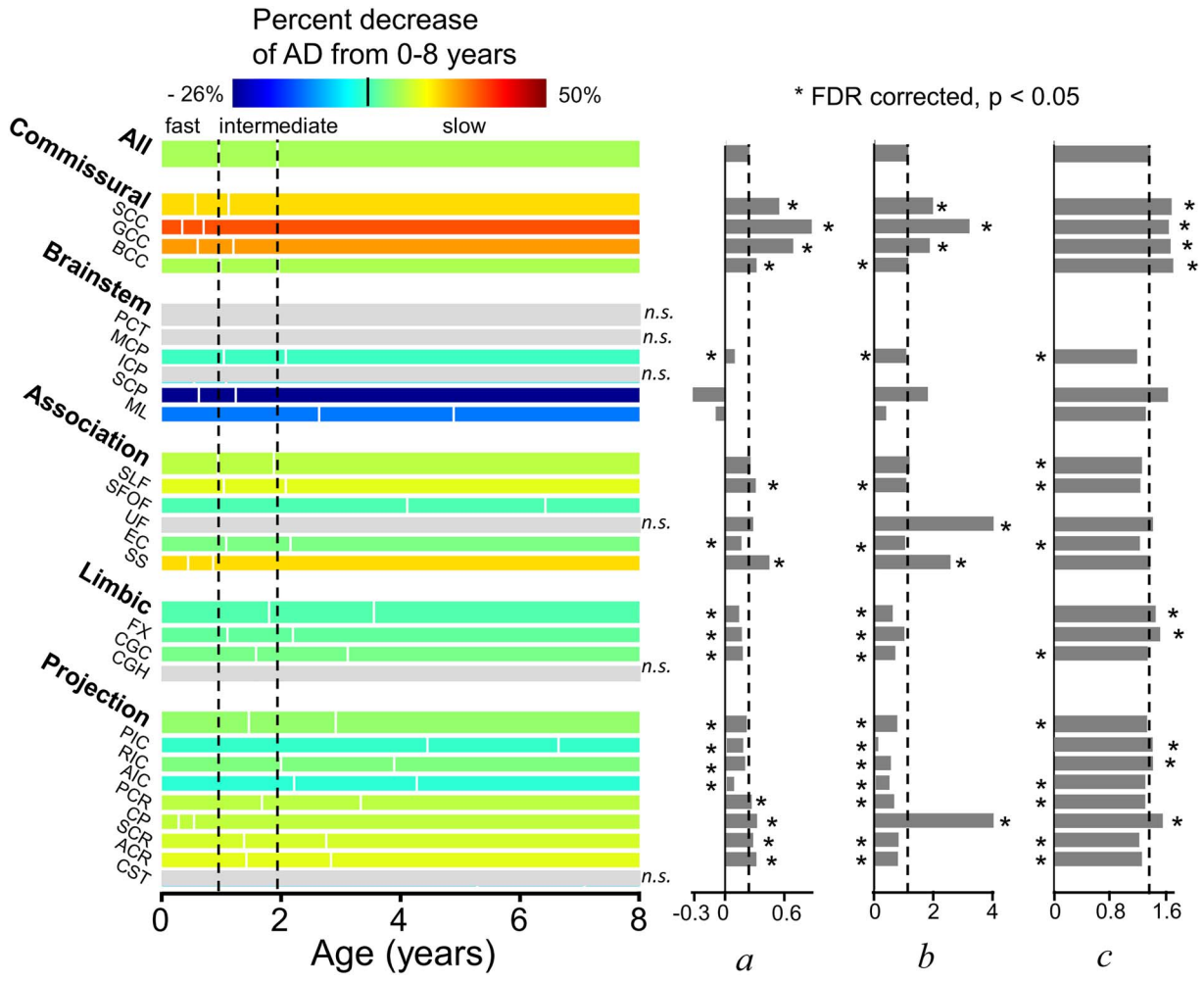

Figure 8. Illustration of percentage increase of AD from 0 to 8 years (with the percentage decrease values listed in Table 1), three phases (with the start/end ages and phase length listed in Table 5) and estimated fitting parameters a, b, and c of exponential curves of AD across all major WM tracts and tract groups. Measures of averaged entire WM were used as the reference. On the left panel, the WM maturation of every WM tract and tract group was displayed in three phases (fast, intermediate, and slow phases), with the boundaries of the three phases of the entire WM displayed as two reference dashed lines. The color bar encodes the percent decreases of AD from 0 to 8 years. * indicates significant difference of a fitting parameter a, b, or c from that of the averaged entire WM, shown as the black dashed lines. * placed on the left side indicates that the fitting parameter a, b, or c is significantly smaller than the entire WM's, and vice versa. With nonsignificant (n.s.) exponential fitting ($R^2 < 0.223$) of AD measurements of PCT, ICP, UF, CGH, CST, and brainstem tract group, the percentage changes of these specific tracts/tract group are not available (shown in gray) and fitting parameters a, b, and c are not shown. Statistical comparisons of the fitting parameters between SCP/ML and those of averaged entire WM were not conducted due to opposite percentage change directions of AD measurements for these two tracts. Please see legend of Figure 1 for abbreviations of WM tract names.

Notes and Conflicts of Interest

The authors would like to thank Samantha Lam at Children's Hospital of Philadelphia for her contribution to writing. The authors report no biomedical financial interests or potential conflicts of interest.

References

Aghajani M, Veer I, van Lang N, Meens P, Van Den Bulk B, Rombouts S, Vermeiren R, Van Der Wee N. 2014. Altered white-matter architecture in treatment-naive adolescents with clinical depression. *Psychological Medicine*. 44:2287–2298.

Alexander AL, Lee JE, Lazar M, Boudos R, DuBray MB, Oakes TR, Miller JN, Lu J, Jeong E-K, McMahon WM. 2007. Diffusion tensor imaging of the corpus callosum in autism. *Neuroimage*. 34:61–73.

Asato M, Terwilliger R, Woo J, Luna B. 2010. White matter development in adolescence: a DTI study. *Cerebral Cortex*. 20:2122–2131.

Barnea-Goraly N, Kwon H, Menon V, Eliez S, Lotspeich L, Reiss AL. 2004. White matter structure in autism: preliminary evidence from diffusion tensor imaging. *Biological Psychiatry*. 55:323–326.

Bashat DB, Kronfeld-Duenias V, Zachor DA, Ekstein PM, Hendler T, Tarrasch R, Even A, Levy Y, Sira LB. 2007. Accelerated maturation of white matter in young children with autism: a high b value DWI study. *Neuroimage*. 37:40–47.

Beaulieu C. 2002. The basis of anisotropic water diffusion in the nervous system–a technical review. *NMR in Biomedicine*. 15:435–455.

Bengtsson SL, Nagy Z, Skare S, Forsman L, Forssberg H, Ullén F. 2005. Extensive piano practicing has regionally specific

effects on white matter development. *Nature Neuroscience*. 8:1148–1150.

Brauer J, Anwander A, Friederici AD. 2011. Neuroanatomical prerequisites for language functions in the maturing brain. *Cerebral Cortex*. 21:459–466.

Brody BA, Kinney HC, Kloman AS, Gilles FH. 1987. Sequence of central nervous system myelination in human infancy. I. An autopsy study of myelination. *Journal of Neuropathology & Experimental Neurology*. 46:283–301.

Carreiras M, Seghier ML, Baquero S, Estévez A, Lozano A, Devlin JT, Price CJ. 2009. An anatomical signature for literacy. *Nature*. 461:983–986.

Clowry G, Molnar Z, Rakic P. 2010. Renewed focus on the developing human neoncortex. *Journal of Anatomy*. 217:276–288.

Cullen KR, Klimes-Dougan B, Muetzel R, Mueller BA, Camchong J, Houri A, Kurma S, Lim KO. 2010. Altered white matter microstructure in adolescents with major depression: a preliminary study. *Journal of the American Academy of Child and Adolescent Psychiatry*. 49:173.

Deoni SC, Dean DC, O'muircheartaigh J, Dirks H, Jerskey BA. 2012. Investigating white matter development in infancy and early childhood using myelin water faction and relaxation time mapping. *Neuroimage*. 63:1038–1053.

Douaud G, Smith S, Jenkinson M, Behrens T, Johansen-Berg H, Vickers J, James S, Voets N, Watkins K, Matthews PM. 2007. Anatomically related grey and white matter abnormalities in adolescent-onset schizophrenia. *Brain*. 130: 2375–2386.

Dubois J, Dehaene-Lambertz G, Perrin M, Mangin JF, Cointepas Y, Duchesnay E, Le Bihan D, Hertz-Pannier L. 2008. Asynchrony of the early maturation of white matter bundles in healthy infants: quantitative landmarks revealed noninvasively by diffusion tensor imaging. *Human Brain Mapping*. 29: 14–27.

Dubois J, Hertz-Pannier L, Dehaene-Lambertz G, Cointepas Y, Le Bihan D. 2006. Assessment of the early organization and maturation of infants' cerebral white matter fiber bundles: a feasibility study using quantitative diffusion tensor imaging and tractography. *Neuroimage*. 30:1121–1132.

Dubois J, Poupon C, Thirion B, Simonnet H, Kulikova S, Leroy F, Hertz-Pannier L, Dehaene-Lambertz G. 2016. Exploring the early organization and maturation of linguistic pathways in the human infant brain. *Cerebral Cortex*. 26: 2283–2298.

Engvig A, Fjell AM, Westlye LT, Moberget T, Sundseth Ø, Larsen VA, Walhovd KB. 2012. Memory training impacts short-term changes in aging white matter: a longitudinal diffusion tensor imaging study. *Human Brain Mapping*. 33:2390–2406.

Frazier JA, Breeze JL, Papadimitriou G, Kennedy DN, Hodge SM, Moore CM, Howard JD, Rohan MP, Caviness VS, Makris N. 2007. White matter abnormalities in children with and at risk for bipolar disorder. *Bipolar Disorders*. 9:799–809.

Gao W, Lin W, Chen Y, Gerig G, Smith JK, Jewells V, Gilmore JH. 2009. Temporal and spatial development of axonal maturation and myelination of white matter in the developing brain. *American Journal of Neuroradiology*. 30:290–296.

Geng X, Gouttard S, Sharma A, Gu H, Styner M, Lin W, Gerig G, Gilmore JH. 2012. Quantitative tract-based white matter development from birth to age 2years. *Neuroimage*. 61:542–557.

Gogtay N, Lu A, Leow AD, Klunder AD, Lee AD, Chavez A, Greenstein D, Giedd JN, Toga AW, Rapoport JL. 2008. Three-dimensional brain growth abnormalities in childhood-onset schizophrenia visualized by using tensor-based morphometry. *Proceedings of the National Academy of Sciences*. 105:15979–15984.

Goodlett CB, Fletcher PT, Gilmore JH, Gerig G. 2009. Group analysis of DTI fiber tracts statistics with application to neurodevelopment. *Neuroimage*. 45:5133–5142.

Hasegawa M, Houdou S, Mito T, Takashima S, Asanuma K, Ohno T. 1992. Development of myelination in the human fetal and infant cerebrum: a myelin basic protein immunohistochemical study. *Brain and Development*. 14:1–6.

Haynes RL, Borenstein NS, Desilva TM, Folkerth RD, Liu LG, Volpe JJ, Kinney HC. 2005. Axonal development in the cerebral white matter of the human fetus and infant. *Journal of Comparative Neurology*. 484:156–167.

Hermoye L, Saint-Martin C, Cosnard G, Lee S-K, Kim J, Nassogne M-C, Menten R, Clapuyt P, Donohue PK, Hua K. 2006. Pediatric diffusion tensor imaging: normal database and observation of the white matter maturation in early childhood. *Neuroimage*. 29:493–504.

Huang H, Fan X, Weiner M, Martin-Cook K, Xiao G, Davis J, Devous M, Rosenberg R, Diaz-Arrastia R. 2012. Distinctive disruption patterns of white matter tracts in Alzheimer's disease with full diffusion tensor characterization. *Neurobiology of Aging*. 33:2029–2045.

Huang H, Fan X, Williamson DE, Rao U. 2011. White matter changes in healthy adolescents at familial risk for unipolar depression: a diffusion tensor imaging study. *Neuropsychopharmacology*. 36:684–691.

Huang H, Xue R, Zhang J, Ren T, Richards LJ, Yarowsky P, Miller MI, Mori S. 2009. Anatomical characterization of human fetal brain development with diffusion tensor magnetic resonance imaging. *Journal of Neuroscience*. 29:4263–4273.

Huang H, Zhang J, Wakana S, Zhang W, Ren T, Richards LJ, Yarowsky P, Donohue P, Graham E, van Zijl PC. 2006. White and gray matter development in human fetal, newborn and pediatric brains. *Neuroimage*. 33:27–38.

Humphreys K, Hasson U, Avidan G, Minshew N, Behrmann M. 2008. Cortical patterns of category-selective activation for faces, places and objects in adults with autism. *Autism Research*. 1:52–63.

Humphreys K, Minshew N, Leonard GL, Behrmann M. 2007. A fine-grained analysis of facial expression processing in high-functioning adults with autism. *Neuropsychologia*. 45:685–695.

Huttenlocher PR. 1990. Morphometric study of human cerebral cortex development. *Neuropsychologia*. 28:517–527.

Hyde KL, Zatorre RJ, Griffiths TD, Lerch JP, Peretz I. 2006. Morphometry of the amusic brain: a two-site study. *Brain*. 129:2562–2570.

Jensen JH, Helpern JA, Ramani A, Lu H, Kaczynski K. 2005. Diffusion kurtosis imaging: the quantification of non-Gaussian water diffusion by means of magnetic resonance imaging. *Magnetic Resonance in Medicine*. 53:1432–1440.

Jiang H, Van Zijl PC, Kim J, Pearlson GD, Mori S. 2006. DtiStudio: resource program for diffusion tensor computation and fiber bundle tracking. *Computer Methods and Programs in Biomedicine*. 81:106–116.

Jones D, Horsfield M, Simmons A. 1999. Optimal strategies for measuring diffusion in anisotropic systems by magnetic resonance imaging. *Magnetic Resonance in Medicine*. 42:515–525.

Kersbergen KJ, Leemans A, Groenendaal F, van der Aa NE, Viergever MA, de Vries LS, Benders MJ. 2014. Microstructural brain development between 30 and 40 weeks corrected age in a longitudinal cohort of extremely preterm infants. *Neuroimage*. 103:214–224.

Kinney HC, Brody BA, Kloman AS, Gilles FH. 1988. Sequence of central nervous system myelination in human infancy: II. Patterns of myelination in autopsied infants. *Journal of Neuropathology & Experimental Neurology*. 47:217–234.

Koldewyn K, Yendiki A, Weigelt S, Gweon H, Julian J, Richardson H, Malloy C, Saxe R, Fischl B, Kanwisher N. 2014. Differences in the right inferior longitudinal fasciculus but no general disruption of white matter tracts in children with autism spectrum disorder. *Proceedings of the National Academy of Sciences*. 111:1981–1986.

Le Bihan D, Mangin JF, Poupon C, Clark CA, Pappata S, Molko N, Chabriat H. 2001. Diffusion tensor imaging: concepts and applications. *Journal of Magnetic Resonance Imaging*. 13:534–546.

Lebel C, Beaulieu C. 2011. Longitudinal development of human brain wiring continues from childhood into adulthood. *Journal of Neuroscience*. 31:10937–10947.

Lebel C, Gee M, Camicioli R, Wieler M, Martin W, Beaulieu C. 2012. Diffusion tensor imaging of white matter tract evolution over the lifespan. *Neuroimage*. 60:340–352.

Lebel C, Treit S, Beaulieu C. 2017. A review of diffusion MRI of typical white matter development from early childhood to young adulthood. *NMR in Biomedicine*. 32: e3778.

Lebel C, Walker L, Leemans A, Phillips L, Beaulieu C. 2008. Microstructural maturation of the human brain from childhood to adulthood. *Neuroimage*. 40:1044–1055.

Leech R, Sharp DJ. 2014. The role of the posterior cingulate cortex in cognition and disease. *Brain*. 137:12–32.

Liston C, Watts R, Tottenham N, Davidson MC, Niogi S, Ulug AM, Casey B. 2006. Frontostriatal microstructure modulates efficient recruitment of cognitive control. *Cerebral Cortex*. 16:553–560.

Mishra V, Guo X, Delgado MR, Huang H. 2015. Toward tract-specifc fractinoal anistropy (TSFA) at crossing-fiber regions with clinical diffusion MRI. *Magnetic Resonance in Medicine*. 74:1768–1779.

Mishra V, Cheng H, Gong G, He Y, Dong Q, Huang H. 2013. Differences of inter-tract correlations between neonates and children around puberty: a study based on microstructural measurements with DTI. *Frontiers in Human Neuroscience*. 7:721.

Mori S, Oishi K, Jiang H, Jiang L, Li X, Akhter K, Hua K, Faria AV, Mahmood A, Woods R. 2008. Stereotaxic white matter atlas based on diffusion tensor imaging in an ICBM template. *Neuroimage*. 40:570–582.

Mukherjee P, Miller JH, Shimony JS, Conturo TE, Lee BC, Almli CR, McKinstry RC. 2001. Normal brain maturation during childhood: developmental trends characterized with diffusion-tensor MR imaging 1. *Radiology*. 221:349–358.

Müller R-A, Kleinhans N, Kemmotsu N, Pierce K, Courchesne E. 2003. Abnormal variability and distribution of functional maps in autism: an FMRI study of visuomotor learning. *American Journal of Psychiatry*. 160:1847–1862.

Nagy Z, Westerberg H, Klingberg T. 2004. Maturation of white matter is associated with the development of cognitive functions during childhood. *Journal of Cognitive Neuroscience*. 16:1227–1233.

Ouyang M, Cheng H, Mishra V, Gong G, Mosconi MW, Sweeney J, Peng Y, Huang H. 2016. Atypical age-dependent effects of autism on white matter microstructure in children of 2–7 years. *Human Brain Mapping*. 37:819–832.

Ouyang M, Dubois J, Yu Q, Mukherjee P, Huang H. 2019a. Delineation of early brain development from fetuses to infants with diffusion MRI and beyond. *NeuroImage*. 185: 836–850.

Ouyang M, Jeon T, Sotiras A, Peng Q, Mishra V, Halovanic C, Chen M, Chalak L, Rollins N, Roberts T, Davatzikos C, Huang H. 2019b. Differential cortical microstructural maturation in the preterm human brain with diffusion kurtosis and tensor imaging. *Proc Natl Acad Sci USA*. 116(10):4671–4680.

Owen MJ, O'Donovan MC, Thapar A, Craddock N. 2011. Neurodevelopmental hypothesis of schizophrenia. *The British Journal of Psychiatry*. 198:173–175.

Petanjek Z, Judas M, Kostovic I, Uylings HB. 2008. Lifespan alterations of basal dendritc trees of pyramidal neurons in the human prefrontal cortex: a layer-specific pattern. *Cereb Cortex*. 18:915–929.

Petanjek Z, Judaš M, Šimić G, Rašin MR, Uylings HB, Rakic P, Kostović I. 2011. Extraordinary neoteny of synaptic spines in the human prefrontal cortex. *Proceedings of the National Academy of Sciences*. 108:13281–13286.

Rakic P, Bourgeois JP, Goldman-Rakic PS. 1994. Synaptic development of the cerebral cortex: implications for learning, memory, and mental illness. *Progress in Brain Research*. 102:227–243.

Rapoport J, Giedd J, Gogtay N. 2012. Neurodevelopmental model of schizophrenia: update 2012. *Molecular Psychiatry*. 17:1228–1238.

Sadeghi N, Nayak A, Walker L, Irfanoglu MO, Albert PS, Pierpaoli C, Group BDC. 2015. Analysis of the contribution of experimental bias, experimental noise, and inter-subject biological variability on the assessment of developmental trajectories in diffusion MRI studies of the brain. *NeuroImage*. 109: 480–492.

Sadeghi N, Prastawa M, Fletcher PT, Wolff J, Gilmore JH, Gerig G. 2013. Regional characterization of longitudinal DT-MRI to study white matter maturation of the early developing brain. *Neuroimage*. 68:236–247.

Schmithorst VJ, Holland SK, Dardzinski BJ. 2008. Developmental differences in white matter architecture between boys and girls. *Human Brain Mapping*. 29:696–710.

Schmithorst VJ, Wilke M, Dardzinski BJ, Holland SK. 2005. Cognitive functions correlate with white matter architecture in a normal pediatric population: a diffusion tensor MRI study. *Human Brain Mapping*. 26:139–147.

Schneider J, Il'yasov K, Hennig J, Martin E. 2004. Fast quantitative diffusion-tensor imaging of cerebral white matter from the neonatal period to adolescence. *Neuroradiology*. 46: 258–266.

Scholz J, Klein MC, Behrens TE, Johansen-Berg H. 2009. Training induces changes in white-matter architecture. *Nature Neuroscience*. 12:1370–1371.

Sedmak D, Hrvoj-Mihić B, Džaja D, Habek N, Uylings HB, Petanjek Z1. 2018. Biphasic dendritic growth of dorsolateral prefrontal cortex associative neurons and early cognitive development. *Croatian Medical Journal*. 59:189–202.

Shenton ME, Dickey CC, Frumin M, McCarley RW. 2001. A review of MRI findings in schizophrenia. *Schizophrenia Research*. 49:1–52.

Silk TJ, Vance A, Rinehart N, Bradshaw JL, Cunnington R. 2009. White-matter abnormalities in attention deficit hyperactivity disorder: a diffusion tensor imaging study. *Human Brain Mapping*. 30:2757–2765.

Simmonds DJ, Hallquist MN, Asato M, Luna B. 2014. Developmental stages and sex differences of white matter and behavioral development through adolescence: a longitudinal diffusion tensor imaging (DTI) study. *Neuroimage*. 92:356–368.

Smith SM, Jenkinson M, Johansen-Berg H, Rueckert D, Nichols TE, Mackay CE, Watkins KE, Ciccarelli O, Cader MZ, Matthews PM. 2006. Tract-based spatial statistics: voxelwise analysis of multi-subject diffusion data. *Neuroimage*. 31:1487–1505.

Song S-K, Sun S-W, Ju W-K, Lin S-J, Cross AH, Neufeld AH. 2003. Diffusion tensor imaging detects and differentiates axon and myelin degeneration in mouse optic nerve after retinal ischemia. *Neuroimage*. 20:1714–1722.

Song S-K, Sun S-W, Ramsbottom MJ, Chang C, Russell J, Cross AH. 2002. Dysmyelination revealed through MRI as increased radial (but unchanged axial) diffusion of water. *Neuroimage*. 17:1429–1436.

Song S-K, Yoshino J, Le TQ, Lin S-J, Sun S-W, Cross AH, Armstrong RC. 2005. Demyelination increases radial diffusivity in corpus callosum of mouse brain. *Neuroimage*. 26:132–140.

Sundaram SK, Kumar A, Makki MI, Behen ME, Chugani HT, Chugani DC. 2008. Diffusion tensor imaging of frontal lobe in autism spectrum disorder. *Cerebral Cortex*. 18: 2659–2665.

Tuch DS, Salat DH, Wisco JJ, Zaleta AK, Hevelone ND, Rosas HD. 2005. Choice reaction time performance correlates with diffusion anisotropy in white matter pathways supporting visuospatial attention. *Proceedings of the National Academy of Sciences of the United States of America*. 102:12212–12217.

Turner LM, Stone WL. 2007. Variability in outcome for children with an ASD diagnosis at age 2. *Journal of Child Psychology and Psychiatry*. 48:793–802.

van Ewijk H, Heslenfeld DJ, Zwiers MP, Faraone SV, Luman M, Hartman CA, Hoekstra PJ, Franke B, Buitelaar JK, Oosterlaan J. 2014. Different mechanisms of white matter abnormalities in attention-deficit/hyperactivity disorder: a diffusion tensor imaging study. *Journal of the American Academy of Child & Adolescent Psychiatry*. 53:790.e793–799.e793.

Wakana S, Jiang H, Nagae-Poetscher LM, Van Zijl PC, Mori S. 2004. Fiber tract–based atlas of human white matter anatomy. *Radiology*. 230:77–87.

Walker L, Gozzi M, Lenroot R, Thurm A, Behseta B, Swedo S, Pierpaoli C. 2012. Diffusion tensor imaging in young children with autism: biological effects and potential confounds. *Biological Psychiatry*. 72:1043–1051.

Weinstein M, Ben-Sira L, Levy Y, Zachor DA, Itzhak EB, Artzi M, Tarrasch R, Eksteine PM, Hendler T, Bashat DB. 2011. Abnormal white matter integrity in young children with autism. *Human Brain Mapping*. 32:534–543.

Westlye LT, Walhovd KB, Dale AM, Bjørnerud A, Due-Tønnessen P, Engvig A, Grydeland H, Tamnes CK, Østby Y, Fjell AM. 2010. Life-span changes of the human brain white matter: diffusion tensor imaging (DTI) and volumetry. *Cerebral Cortex*. 20:2055–2068.

Yakovlev PI, Lecours AR. 1967. The myelogenetic cycles of regional maturation of the brain. In: Minkowski A, editor. *Regional development of the brain in early life*. Oxford: Blackwell, pp. 3–70.

Yu Q, Ouyang A, Chalak L, Jeon T, Chia J, Mishra V, Sivarajan M, Jackson G, Rollins N, Liu S, Huang H. 2016. Structural development of human fetal and preterm brain cortical plate based on population-averaged templates. *Cerebral Cortex*. 26:4381–4391.

Yu Q, Peng Y, Mishra V, Ouyang A, Li H, Zhang H, Chen M, Liu S, Huang H. 2014. Microstructure, length, and connection of limbic tracts in normal human brain development. *Frontiers in Aging Neuroscience*. 6:228.

Zhang H, Schneider T, Wheeler-Kingshott CA, Alexander DC. 2012. NODDI: practical in vivo neurite orientation dispersion and density imaging of the human brain. *Neuroimage*. 61:1000–1016.